IOP Publishing and International Atomic Energy Agency Nuclear Fusion
Nucl. Fusion **52** (2012) 103022 (10pp) doi:10.1088/0029-5515/52/10/103022

Measurements of fast-ion transport by mode-particle resonances on DIII-D

C.M. Muscatello[1], B.A. Grierson[2], R.W. Harvey[3], W.W. Heidbrink[1], D.C. Pace[4] and M.A. Van Zeeland[4]

[1] Department of Physics and Astronomy, University of California, Irvine, CA 92697, USA
[2] Princeton Plasma Physics Laboratory, Princeton, NJ 08543, USA
[3] CompX, Del Mar, CA 92014, USA
[4] General Atomics, San Diego, CA 92186, USA

Received 16 May 2012, accepted for publication 5 September 2012
Published 24 September 2012
Online at stacks.iop.org/NF/52/103022

Abstract
Magnetohydrodynamic (MHD) instabilities in tokamak plasmas manifest in a variety of ways, characterized by different scale lengths and mode frequencies. MHD activity can cause significant degradation of plasma performance due to transport of particles, energy and current. Among the many different types of MHD, arguably fishbones, sawteeth and Alfvén eigenmodes (AEs) are observed to cause the largest fluxes of superthermal ions. DIII-D's expansive suite of diagnostics makes it possible to rigorously characterize these instabilities and study their interaction with fast ions. This review paper first presents an overview of the recent additions to DIII-D's collection of fast-ion diagnostics. The extended diagnostic capabilities are employed in a series of experiments to investigate fast-ion dynamics in the presence of fishbones, sawteeth and AEs. Results from these seemingly unrelated studies are highlighted, and they reveal that mode-particle resonances play the central role in the observed deterioration of fast-ion confinement.

(Some figures may appear in colour only in the online journal)

1. Introduction

Tokamak plasmas are prone to a variety of instabilities that can degrade particle and energy confinement. Ultimately, reactor-relevant machines like ITER will strive to achieve a burning plasma within the operable capacity of the tokamak. A burning plasma is one whose generated power balances lost power without the use of external power sources. In other words, the fusion power must balance particle and energy losses in order to have sustained burn. Looking forward to burning deuterium–tritium plasmas, the main source of heating results from the energy transfer from the fusion-born energetic alpha particles to the plasma. Instabilities can interact with the energetic alpha particles, potentially leading to degradation in their confinement and their heating efficiency. Before ignition can be achieved, substantial heating from external sources will be required to produce necessarily high plasma temperatures. Two of the proposed techniques planned for ITER are neutral-beam injection (NBI) and ion cyclotron resonant frequency (ICRF) heating. In either case, a superthermal population of ions is created which must be confined long enough to transfer its energy to the plasma. Naturally, an important aspect of tokamak plasmas is an understanding of the physics of the interaction between instabilities and the superthermal ion populations generated through fusion reactions and auxiliary heating schemes.

Some of the most important interactions with energetic particles arise from magnetohydrodynamic (MHD) instabilities, many of which possess wave-like properties. Due to the coherent periodic structure of the electromagnetic fields associated with such instabilities, resonances between a charged particle and electromagnetic waves can cause significant modifications to the unperturbed orbit [1]. According to the Hamiltonian formalism, in toroidal geometry with ζ and θ as the torodial and poloidal angular coordinates of the particle, n and m as the toroidal and poloidal mode numbers, and ω as the frequency of the mode, exact resonance occurs when the phase change between the mode and particle is zero (i.e. $n\,\mathrm{d}\zeta/\mathrm{d}t - m\,\mathrm{d}\theta/\mathrm{d}t - \omega = 0$). For well-passing particles with small orbit width, it is possible to satisfy this zero-phase change condition along the entire orbit. However, for particles with finite orbit width, their trajectories become increasingly complicated. Instead, a resonance is possible if the phase change integrates to zero after a bounce period. The so-called bounce-precessional resonance can occur for a trapped (passing) charged particle when its bounce (poloidal transit) frequency ω_b and toroidal precession (transit) frequency ω_pr satisfy

$$\omega - s\omega_\mathrm{b} - n\omega_\mathrm{pr} = 0, \tag{1}$$

where s is an integer. Because of the widely different fast-ion orbits, instabilities with a variety of frequencies

and mode structures can lead to coherent resonances with energetic ions.

On the PDX tokamak, observations of large beam-ion losses concurrent with bursts of MHD activity dubbed 'fishbones' [2] spurred theoretical investigations as to the cause of the large losses. The traditional fishbone instability appears in high-beta plasmas with a $q = 1$ surface where a sufficiently large trapped particle population destabilizes the $m/n = 1/1$ internal kink mode [3]. The observed ejection of beam ions during a fishbone burst can be explained by 'particle pumping' resonance, where the mode frequency matches the toroidal precession frequency of trapped beam ions [4].

On the other hand, plasmas with low to moderate fast ion pressure and $q < 1$ are susceptible to periodic collapsing of plasma density and temperature due to the sawtooth instability. Various fluctuations diagnostics, such as magnetics, soft x-ray and electron temperature measurements, suggest that rearrangement of the core flux surfaces takes place during the collapse phase. Observations on JET show redistribution of ICRF-heated helium-3 minority ions at a sawtooth crash [5]. The conventional theory of transport by flux attachment [6] cannot explain the observed redistribution of the highly energetic helium ions. One theory details a possible transport mechanism, attributing it to resonant matching of the mode frequency to the characteristic orbital bounce and precession frequencies [7].

On the DIII-D tokamak, large beam-ion losses are observed concurrently with bursts of MHD activity attributed to toroidicity-induced Alfvén eigenmodes (TAE) [8]. TAE-induced losses have also been observed on JET and ASDEX-Upgrade [9–11]. Similar to the fast-ion losses by fishbones and sawteeth, the TAE-induced losses are explained in terms of particles phase-locking with the mode and experiencing convective losses due to outward $E \times B$ drifts.

Magnetic islands, often referred to as tearing modes in tokamak plasmas, can also lead to redistribution and loss of energetic particles. While orbit stochasticity has been identified as the ultimate cause of the transport [12, 13], the stochasticity is fundamentally a result of multiple mode-particle resonances due to multiple overlapping islands [14]. We note, however, that current work on tearing-mode-induced fast-ion transport in DIII-D is ongoing, and a detailed discussion will be deferred to a future publication.

These historic observations of fishbones, sawteeth and Alfvén eigenmodes (AEs) have motivated extensive experimental and theoretical investigations regarding fast-ion interactions with instabilities on a variety of magnetic confinement systems. It is the purpose of this paper to highlight the latest diagnostic improvements and advances in our understanding of fast-ion transport by these MHD instabilities in the DIII-D tokamak. The paper is organized as follows: section 2 provides an overview to the recent additions to the fast-ion diagnostic suite on DIII-D. Sections 3, 4 and 5 review the results from three independent studies of fast-ion transport during fishbones, sawteeth and AEs, respectively. Finally, summarizing comments can be found in section 6.

2. New fast-ion diagnostics on DIII-D

DIII-D has extensive diagnostic capabilities, and recent additions to its fast-ion diagnostic suite over the past few years have led to various advances in the physics of energetic particles. Fast-ion deuterium-alpha (FIDA) is a spectroscopic technique that exploits the charge-exchange process between energetic deuterium ions and neutral-beam injected deuterons [15, 16]. A re-neutralized fast ion has the probability of becoming atomically excited either through the charge-exchange process or through collisions with the bulk plasma. An excited hydrogen atom that undergoes the atomic transition from $n = 3 \rightarrow 2$ will emit a photon at the familiar Balmer-α (or Dα in the case of deuterium) wavelength. The Dα wavelength of the emitted photon in the particle's frame of reference is $\lambda_0 =$ 656.1 nm. However, because of the superthermal velocity of the re-neutral, the wavelength of the emitted photon is Doppler-shifted in the lab frame. Consequently, the Dα spectrum is modified with a broad low-intensity feature in the presence of a fast deuterium population (see figure 1). This broad feature, typically consisting of blue- and red-shifted wings about λ_0, is the subject of investigation for FIDA. One should then be able to measure the FIDA component of the Dα spectrum and extract some information about the velocity distribution of the energetic deuterium population. In ideal conditions, the FIDA contribution is simply the difference between an active measurement (neutral beam on) and a passive measurement (neutral beam off). In practice however extraction of the fast-ion feature from the Dα spectrum is more complicated; details regarding the subtleties of FIDA analysis can be found in [16], and a detailed application of FIDA analysis to sawtooth-induced fast-ion redistribution in [17].

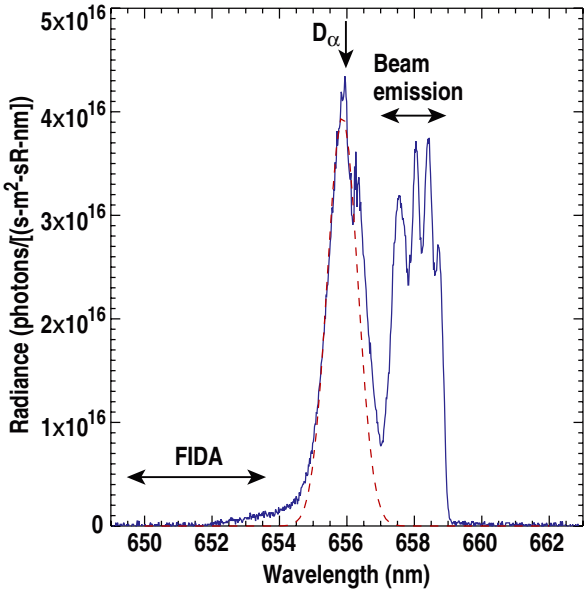

Figure 1. Full Dα spectrum (solid) showing the main ion, beam emission and FIDA components. Gaussian-fitted main deuterium ion contribution (dashed).

A prototype study of the FIDA technique on DIII-D was achieved by tuning some of the spectrometers from the charge-exchange recombination (CER) diagnostic to the FIDA portion of the Dα spectrum [15]. The success of this technique led to DIII-D's dedicated 1st generation FIDA spectrometer [18], which collects signal from two radial channels and shares the same optical installation with an earlier installed CER system. The optical fibres are installed near the bottom of the

tokamak and are situated to view (nearly perpendicularly) one of DIII-D's co-current tangentially injecting neutral beams. Although only two vertically viewing fibres are dedicated to FIDA, the option is available to tune the CER spectrometers to FIDA for full spatial coverage.

The ability to derive useful physics from the 1st generation FIDA diagnostic motivated the conceptual design [19] and implementation [20] of the 2nd generation FIDA system on DIII-D. This second incarnation of FIDA differs in several ways from its 1st generation predecessor. Among the differences, the most important include the viewing geometry and spatial coverage. The tokamak optical components are located near the top of the tokamak, and the sightlines intersect one of DIII-D's counter-current tangentially injecting neutral beams. The sightlines intersect the neutral beam obliquely, having comparable vertical and toroidal components. The fibres collect light from 11 radial positions along the neutral beam (typically from the magnetic axis to $r/a \sim 0.8$) as well as three radial positions displaced toroidally away from the beam. These three passive channels allow continual monitoring of the background signal without the use of beam modulation. Although 11 active channels exist, due to spatial and spectral resolution constraints of the FIDA spectrometer, spectral data from only six channels are recorded during a single discharge. A patch panel allows the user to swap fibres for full spatial coverage with a repeat shot. In addition to the 2nd generation FIDA spectrometer (s-FIDA), a high-bandwidth FIDA system (f-FIDA) was also installed in 2010 [20]. Light from six radial channels pass through a narrowband interference filter centred at a moderate Doppler shift on the blue wing of the Dα spectrum. The filter is mounted in a rotatable stage allowing one to adjust the bandpass region according to the desired spectral energy range. A photomultiplier tube (PMT) integrates the light passed through the filter, and the output is amplified and digitized at 1 MHz. A sensitivity study shows that signal to noise is high for fluctuations up to about 100 kHz.

The third incarnation of FIDA on DIII-D is an imaging system providing two-dimensional spatial profiles of the FIDA emission [21]. A fast framing camera, in conjunction with a narrowband interference filter, images the 2D spatial structure of FIDA emission from fast ions undergoing charge exchange with one of DIII-D's co-current tangentially injecting neutral beams. The imaging system is essentially a collection of individual viewing chords (like the aforementioned 1D FIDA systems) corresponding to the pixels of a two-dimensional imaging array. The camera views the neutral beam in the midplane, and the 'sightlines' are approximately tangential to the magnetic field.

The most recent addition to DIII-D's FIDA suite is the installation of 16 channels, eight of which view one of DIII-D's co-current injecting neutral beams and eight of which view one of DIII-D's counter-current injecting neutral beams [22, 23]. The fibres are arranged in the midplane and possess a tangential viewing geometry. The spectrometer measures the full Dα spectrum up to large Doppler shifts simultaneously for all 16 channels with the primary goal of determining the thermal ion temperature and toroidal rotation. Although the FIDA feature is lower intensity than the thermal ion and beam-emission contributions to the spectrum by as much as two orders of magnitude, it is well-resolved using the high-gain setting of the diagnostic. Only recently available in 2011, the 16-channel system was not yet in use for the experiments whose data are discussed later.

The advantage of having multiple optical installations for FIDA measurements extends beyond added spatial coverage; different viewing geometries probe different regions of velocity space. The unique sightlines of each of the four DIII-D FIDA systems are sensitive to different classes of particles. The more vertically viewing sightlines tend to weigh heavily the portions of velocity space dominated by trapped particles, while the more tangentially viewing sightlines more heavily weigh the passing particle regions. With the collective information from each of the FIDA systems, one can discriminate the dynamics of fast ions by orbit type. Details regarding the calculation of the velocity-space sensitivity of FIDA can be found in [24], and a comparison of the sensitivities for different optical installations can be found in [17].

In addition to confined fast-ion measurements, DIII-D also has a collection of detectors for measuring losses. Among them, the scintillator-based fast-ion loss detectors (FILDs) are capable of resolving the pitch-angle and energy distribution of fast deuterium ions lost from the plasma. The concept is based on a similar FILD diagnostic on ASDEX Upgrade [25] which was adopted from an earlier scintillator-based loss detector on TFTR [26]. The design resembles a magnetic spectrometer, discriminating particles by pitch angle and gyroradius (energy). The detector is located within the outer wall of the vessel and accepts gyrating fast ions through a slit aperture, whose size determines the pitch angle and energy resolution. Particles entering the aperture with different pitch angles and energy strike and illuminate different regions of the scintillator detector face. The scintillator is imaged by a charge-coupled device (CCD) camera, and a post-processing routine maps a pitch angle and energy grid to the recorded image. High-bandwidth signals (>100 kHz) are also obtained simultaneously by integrating the light over a region of the scintillator using a PMT. The first implementation on DIII-D (FILD 1) is installed 45° below the midplane and accepts fast ions travelling in the usual direction of the plasma current (counterclockwise viewed from the top of the tokamak) [27, 28]. The second implementation (FILD 2), also accepting fast ions travelling in the direction of the plasma current, is installed at the midplane separated toroidally by 60° from FILD 1. Available in 2011, FILD 2 was not yet in use during the experiments whose data are discussed later.

These recent additions to the DIII-D fast-ion diagnostic suite complement the numerous existing diagnostics, such as neutron detectors [29], neutral particle analysers (NPAs) [30] and Faraday-cup beam-ion loss detectors (BILDs) [31]. Several fast-ion experiments during the 2010 DIII-D experimental campaign were performed employing DIII-D's collection of fast-ion diagnostics available at that time. In the following, highlights from these experiments will be presented in the form of a review of DIII-D studies that focus on fast-ion transport phenomena during fishbones and AEs. In addition, a unique discharge on DIII-D shows compelling evidence of resonant transport of fast ions at a sawtooth crash. Although superficially these three instabilities may seem disparate, they are closely related through the mechanism by which they drive fast-ion transport, namely wave-particle resonances.

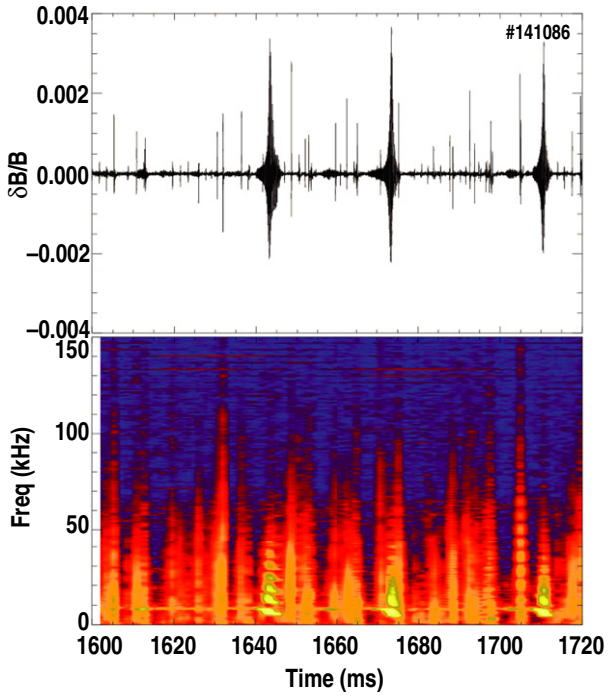

Figure 2. Time history of (*a*) external magnetic probe during three off-axis fishbone bursts and (*b*) crosspower of two magnetic probes separated toroidally.

3. Off-axis fishbones on DIII-D

Bursts, similar to traditional $q = 1$ fishbones, are observed on DIII-D in high-beta plasmas with $q > 1$ and heated by NBI [32, 33]. Dubbed 'off-axis fisbones,' they have a fishbone-like magnetic signal and eigenfunction situated on the $q = 2$ surface. The bursts, each lasting about 2 ms and occurring periodically approximately every 20 ms, possess a downward-chirping frequency spectrum. The characteristic magnetic signal of three off-axis fishbone bursts is presented in figure 2(*a*). The signal is obtained from a magnetic probe located within the outer wall at the midplane. The crosspower between two magnetic probes separated toroidally at the midplane is shown in figure 2(*b*). The spectral features of the burst near $t = 1640$ ms are well resolved and show multiple harmonics. The fundamental $n = 1$ component has a frequency of about 6 kHz. For fishbones characterized by $n = 1$ and relatively low frequency [O(10 kHz)], the mode-particle resonance occurs when a trapped particle's toroidal precession frequency matches the mode frequency,

$$\omega = \omega_{\mathrm{pr}} \tag{2}$$

Resonance with passing particles is also possible and occurs for mode frequencies well below the transit frequency. In general, however, resonances with passing particles is less important since the spatial range over which the resonance condition is satisfied is small [4]. The magnetic perturbations produced during fishbone bursts lead to periodic and secular modifications to particle orbits. For a resonant particle, the secular motion dominates and, over the course of each bounce period, the particle gets kicked in the radial direction. Figure 3 depicts the resonance condition (equation (2)) in velocity space

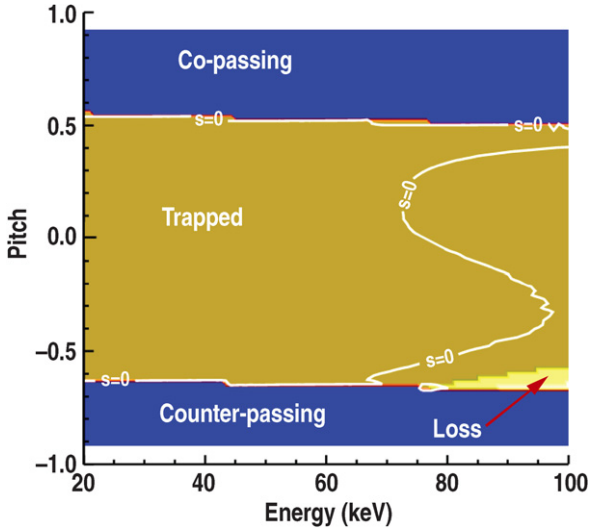

Figure 3. Velocity-space plot of orbit classification and primary resonance curve pertaining to off-axis fishbone mode ($n = 1$; $f = 6$ kHz), evaluated on the $q = 2$ surface at the midplane.

near the $q = 2$ surface during the fishbone burst around $t = 1640$ ms. The definition of pitch used in figure 3 and the remainder of this paper is the local value of $v_{\parallel}/v$. Trapped particles near the NBI energy (80 keV) have the greatest potential for loss. Particles with orbits satisfying equation (2) can lose/gain energy and canonical toroidal momentum during the resonant interaction, leading to an orbit transformation into the lost region of velocity space.

Off-axis fishbone-induced losses of beam ions are observed in seven independent detectors, including a novel implementation of DIII-D's FIDA and beam-emission spectroscopy (BES) systems [34]. The primary goal of the FIDA diagnostic is to measure the Doppler shift of photons emitted from atomically excited neutralized fast ions that undergo charge exchange with injected beam neutrals [15]. However, when used passively (the diagnostic neutral beam turned off), the FIDA diagnostic can detect lost fast ions that undergo charge exchange with edge neutrals, assuming the efflux of fast ions and edge neutral density are large enough to produce sufficient light. The BES diagnostic measures density fluctuations through detection of the emitted light from injected neutrals excited by collisions with the bulk plasma [35]. The DIII-D BES system measures the Doppler-shifted beam-emission components of the D-alpha spectrum (see figure 1) to diagnose density fluctuations [36]. Therefore, with the neutral beam off in passive mode, it too can pick-up FIDA light emitted from the edge. Data from the seven loss detectors provide corroborating evidence that losses are emitted in a beacon-like fashion with a fixed phase relative to the mode, just like the losses observed on PDX. Analysis of a database of 513 bursts with $n = 1$ structure in $q > 1$ plasmas was compiled. The beam-ion loss rate at each burst is assessed by the time derivative of the neutron rate. The mode amplitude at each burst is determined from $\mathrm{d}B/\mathrm{d}t$ measured by an external magnetic probe. Similar to the losses on PDX during $q = 1$ fishbone bursts, the beam-ion loss rate and the mode amplitude correlate well (Pearson linear correlation coefficient $r = 0.81$, where $r = 0$ is no correlation and $r = 1$ is perfect linear

correlation) during off-axis fishbone bursts. Theoretically, linear dependence of the loss rate on the mode amplitude indicates convective transport mechanism. Diffusive transport cannot be ruled-out, however, since the beam-ion loss rate also correlates well with the square of the mode amplitude. However, the coherence of the losses with the mode and the comparable nature of fast-ion losses observed in both types of fishbones on PDX and DIII-D suggests that the same resonance-induced convective loss mechanism applies. The interested reader is referred to [34] for detailed characterization of off-axis fishbones and their interaction with energetic beam ions.

4. Sawteeth on DIII-D

Observations of fast-ion transport at a sawtooth crash have been observed on virtually every major tokamak. According to one theory, transport of energetic particles during the crash depends on their energy and pitch angle [37]. The FIDA diagnostic samples a finite swath of velocity space. Each of the FIDA installations at DIII-D resolves a different region of energy and pitch angle. FIDA data in NBI-heated discharges at DIII-D are consistent with the theoretical expectation that transport of fast ions is pitch angle and energy dependent [17]. Furthermore, the data are in agreement with the explanation that the redistribution is associated with particle attachment to the evolving flux surfaces, but strong toroidal drift (possessed dominantly by trapped ions) can decouple the particle from the perturbed evolving flux surfaces. Higher energies lead to higher drift velocities, and a critical energy (E_{crit}) exists at which fast ions are uninfluenced by the perturbed flux surfaces over the duration of the crash. That is, if the mode evolves slowly over a toroidal orbital period, the particle's 3rd adiabatic invariant is nearly conserved, and it remains close to its unperturbed drift surface. Therefore, it might be expected that sufficiently energetic ions are impervious to redistribution by sawteeth. However, even fast ions with energy greater than E_{crit} can coherently interact with the 1/1 helical mode associated with the sawtooth crash through mode-particle resonances [7, 38]. A sufficient condition for the *possibility* of resonance is that the helical mode persists for several toroidal periods of the particle; otherwise, the transport is explained by the aforementioned flux-attachment description. Of course, an additional requirement for effective transport by the resonance is that the amplitude of the helical perturbation is sufficiently large, since such convective transport scales linearly with the mode amplitude.

Experiments on DIII-D show preliminary evidence of mode-particle resonances at a sawtooth crash. The plasma shot of interest is #141196, an L-mode discharge with both NBI and ICRF heating at the tail-end of the discharge. Before the ICRF is turned on, during NBI only, the line-averaged electron density is $2.3 \times 10^{19}\ \mathrm{m}^{-3}$ and central electron temperature is 2.8 keV. When 2.5 MW of ICRF heating is included (1.1 MW at 60 MHz and 1.4 MW at 90 MHz, corresponding to the 4th and 6th harmonics of the deuterium ion cyclotron frequency), the line-averaged density increases to $3.3 \times 10^{19}\ \mathrm{m}^{-3}$, central electron temperature rises to 5.3 keV, and the neutron rate increases by a factor of 1.94. To test whether the increase in the measured neutron rate with ICRF is a result of the increased slowing-down time of the beam ions, or whether the neutron rate rises due to ICRF damping on and acceleration of beam ions, we perform a transport analysis with the TRANSP code [39] over the duration of the three heating phases of this discharge (NBI only, NBI+60 MHz ICRF and NBI+60+90 MHz ICRF). In this analysis, while the time-varying measured plasma profiles and EFIT [40] equilibria are used, TRANSP is set up to treat only heating and particle fuelling by NBI (via the NUBEAM module [41]). The agreement between the measured neutron rate and that predicted by TRANSP during the NBI-only phase is excellent. The agreement worsens during the ICRF phases; during the NBI+60+90 MHz heating phase, the neutron rate predicted by TRANSP increases by a factor of 1.79 greater than the value during NBI only, compared with the factor of 1.94 increase seen experimentally. The rise in the neutron rate predicted by TRANSP is a result of the increased slowing-down time of the beam ions; with the values quoted above for T_{e} and n_e, one can see that

$$\frac{\tau_2}{\tau_1} = \left(\frac{T_2}{T_1}\right)^{3/2} \left(\frac{n_1}{n_2}\right) \approx 1.81.$$

However, we claim that the deficit in the neutron rate predicted by TRANSP, compared with the experimental value, is a result of the missing heating contribution from ICRF-accelerated beam ions.

Corroborating evidence of FW coupling to the beam ions is seen in both the lengthening of the sawtooth period and the peaking of a radially localized group of beam ions, manifested as an off-axis peak in the fast-ion density profile measured by FIDA. Early experiments on JET showed that, in discharges with high-power ICRF heating, the sawtooth period can be extended up to several seconds [42]. Years later, similar observations were made on DIII-D with lower ICRF power [43, 44]. The lengthening of the sawtooth period is a result of the stabilizing effect of the energetic-ion population on the kink instability (see [45] and references therein). Perhaps the most convincing observation of beam-ion acceleration by ICRF is the appearance of an off-axis peak seen in the fast-ion density profile measured by the vertically viewing FIDA system, which is sensitive mainly to trapped particles. Figure 4 displays the precrash and postcrash spectra measured by vertical FIDA at the midplane, averaged over four sawtooth crashes during the 60+90 MHz ICRF phase. Because the NBI power is low, the FIDA data are noisy. The spectra are integrated over the wavelength range 650.4–651.3 nm, and the integrated values are divided by the local value of the neutral density to yield a quantity that is approximately proportional to the fast-ion density. The profile is plotted in figure 5, and one can readily see the secondary peak at $R = 193$ cm which is absent without ICRF. Similar observations have been reported in earlier DIII-D experiments during 5th and 6th harmonic ICRF heating [24]; the off-axis peak is attributed to the finite orbit-width trapped ions whose banana tips couple to the resonance layer located at the major radius of the magnetic axis. This ICRF-coupling to a narrow group of trapped ions is corroborated by the obliquely viewing FIDA system (sensitive mainly to passing particles), where the shape of the profile is relatively unchanged with and without ICRF.

At a sawtooth crash, the on- and off-axis peaks in the fast-ion density profile are flattened. Furthermore, enhanced signal

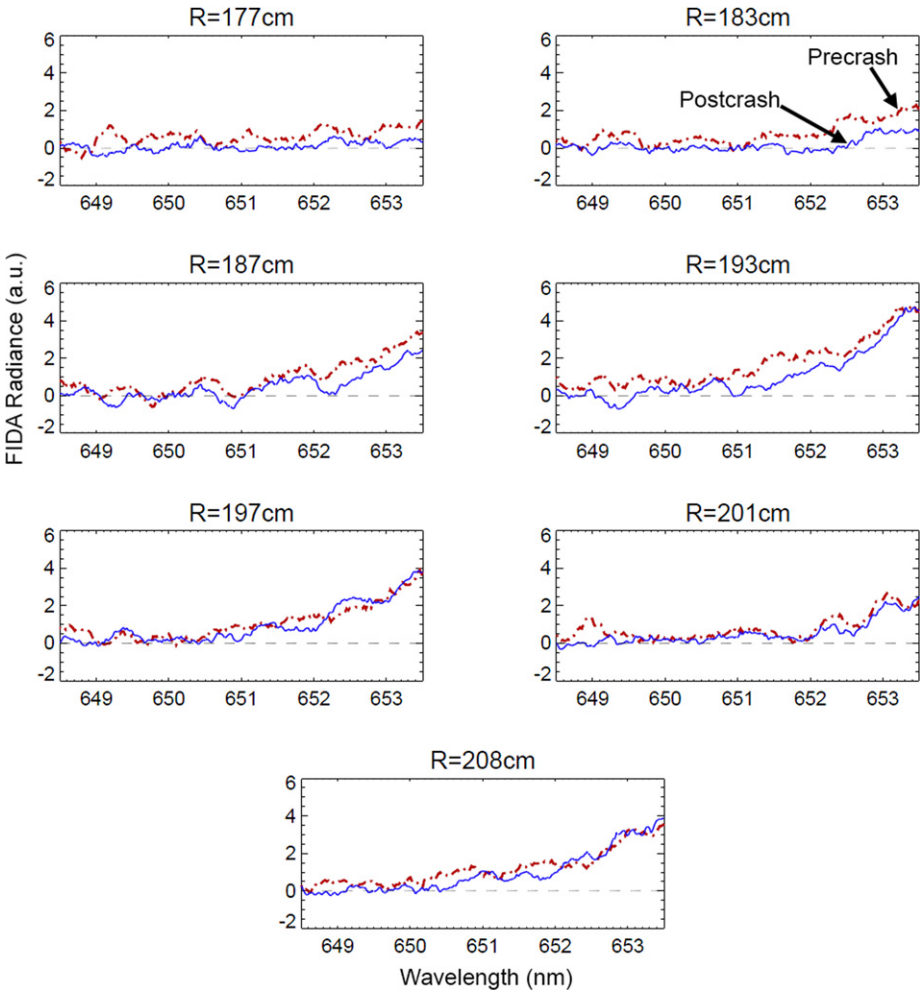

Figure 4. Average precrash and postcrash FIDA spectra for seven channels of the vertical system.

measured by a Faraday-cup FILD appears concurrently with a sawtooth crash and only appears when the ICRF heating is on. The RF-coupled beam ions are measurably influenced by the MHD mode at the sawtooth crash, despite their high energy. Figure 6(*a*) is a time slice of the electron temperature signal measured by the core-most channel of the electron-cyclotron emission (ECE) radiometer [46]. The sawtooth characteristic is readily seen; the large drops in T_e correspond to the sawtooth crashes, accompanied by bursts in signal measured by external magnetic coils (figure 6(*c*)). Also plotted in figure 6(*a*), the ICRF power coupled to the plasma injected by the fast-wave antennae is shown. The plasma is heated by NBI alone until $t = 4350$ ms when the 60 MHz fast-wave system is initiated. Then at $t = 4700$ ms, the 90 MHz fast-wave antenna is also energized and further heating is achieved, evidenced by the increasing amplitude and period of the sawtooth cycles. The fast-ion loss signal in figure 6(*b*) arises from ions with energy greater than 10 keV striking the Faraday-cup detector on the outer wall at the midplane. Enhancements in the loss signal occur at a sawtooth crash only when the ICRF is on, and the enhancements are slightly more pronounced during the 60+90 MHz ICRF phase (26% increase) compared with the 60 MHz-only phase (22% increase). The appearance of these modest loss signals with ICRF suggests the possibility of a narrow coupling between the radially localized RF-accelerated beam ions and the MHD mode at the sawtooth crash.

Assessment of the transport requires knowledge of (1) the regions of velocity space affected by the sawtooth instability and (2) the velocity-space distribution of fast ions just before a crash. To determine the regions of velocity space affected by the sawtooth crash, equation (1) is evaluated. Since its first observations, despite the disparity in the proposed details of the mode growth and thermal collapse phase, the sawtooth instability is virtually always described by the existence of an $m/n = 1/1$ mode [47–50], routinely observed before and/or after the thermal crash with various fluctuation diagnostics [51, 52] at a frequency comparable to the toroidal rotation of the plasma [53]. Recent observations on ASDEX-Upgrade and DIII-D identify the existence of a low-frequency sawtooth precursor (LFSP) [52, 53] that may play a role in the thermal crash [52]. Although the frequency of the dominant 1/1 precursor is not a rational value of the LFSP, the LFSP is thought to be also a 1/1 mode. This inharmonic nature of the 1/1 mode leads to harmonic distortion resulting in overtones of integer multiples of the fundamental frequency (i.e. harmonics of the 1/1, e.g. 2/2, 3/3, etc). The 1/1 harmonics are readily seen in spectrograms of various fluctuation diagnostics and are also observed in our DIII-D discharge (see figure 6(*d*).

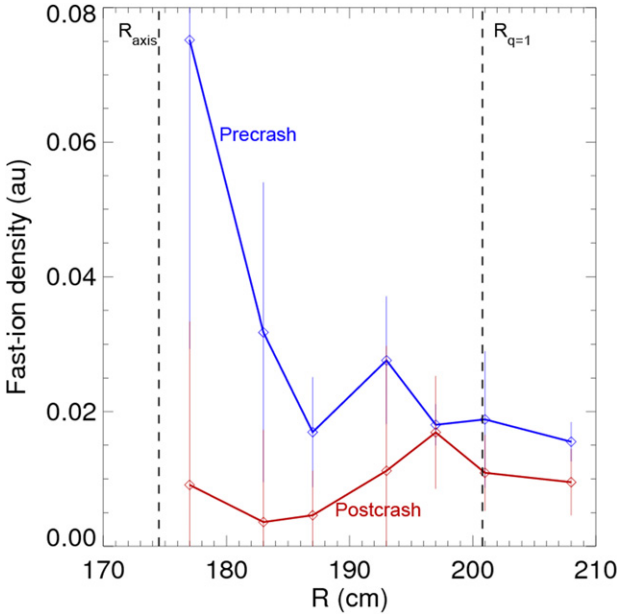

Figure 5. Average precrash and postcrash fast-ion density profiles versus major radius at the midplane. The locations of the magnetic axis and the $q = 1$ surface, determined by equilibrium reconstructions, are denoted.

Since the 1/1 harmonics are by far the dominant modes present adjacent a sawtooth crash, we address the issue of fast-ion resonances with these harmonics. The 1/1 mode frequency ω is determined by the plasma toroidal rotation which depends on the equilibrium electric field [38]. The frequency of the fundamental 1/1 harmonic is ∼6 kHz (determined from the spectrogram in figure 6(*d*)) which matches the plasma toroidal rotation inside the $q = 1$ surface, determined by CER measurements. Higher harmonics (2/2 and sometimes 3/3) are also present.

In figure 7, two velocity space maps are presented along with the relevant resonance curves (solid curves) and the critical energy boundary ($E_{\rm crit}$, dashed curve). The velocity-space maps are calculated at the off-axis position where ICRF enhances the trapped fast-ion profile (midplane at $R = 193$ cm). Figure 7(*a*) denotes orbit boundaries calculated by a single-particle guiding-centre code (appendix of [54]), and figure 7(*b*) depicts an estimate of the fast-ion distribution function during the NBI+ICRF heating phase. The distribution function is modelled with the quasi-linear Fokker–Planck code CQL3D [55] coupled to the ray tracing code GENRAY [56]. The effect of the ICRF heating on the beam-ion distribution is readily seen. The full-energy components of the co- and counter-current injecting neutral beams correspond to the local peaks in the distribution function at $E = 75$ keV and pitch values of about −0.6 (for the counter-source) and +0.6 (for the co-source). The CQL3D simulation shows clear acceleration by ICRF heating of (mainly poloidally trapped) beam ions above the NBI energy into the region where the $s > 0$ resonances become non-degenerate. For the $s = 0$ resonant particles, the mode frequency and the toroidal precession are nearly equal, and the particles are phase-locked to the mode (just like the primary fishbone resonance). This resonance primarily affects well-trapped and marginally trapped ions with $E < 80$ keV, mainly beam ions. For $E > 80$ keV, the $s > 0$ resonances begin to spread-out and encompass more of velocity space, overlapping the ICRF-accelerated beam ions.

The fast ions contributing to the off-axis peak ($R = 193$ cm) in figure 5 are mainly composed of trapped particles with $E > 50$ keV and $|\text{pitch}| < 0.5$. This portion of velocity space is mainly above the critical energy ($E > E_{\rm crit}$), and the fast ions in this region correspond to those accelerated by ICRF, according to our CQL3D calculations. It is reasonable to conclude that these fast ions exceeding $E_{\rm crit}$ and overlapping the resonant regions of velocity space are contributing to the observed losses in figure 6. Because the sampling time of our s-FIDA data is 1 ms and since we sample several sawtooth cycles, it is not possible to determine when (with better than millisecond accuracy), with respect to the crash, the transport occurs. That which is clear from the data is the fact that a sawtooth crash triggers transport of fast ions. Furthermore, the data presented here suggest that even highly energetic fast ions above $E_{\rm crit}$ (i.e. those that do not follow the perturbed flux surfaces) are susceptible to redistribution and loss.

With that said, the shot shown in figures 4–7 is unique; over the course of the experiment, the plasma shape of the various discharges was swapped between oval and bean-like shapes, and the ICRF power was increased over the course of the experiment. The shot analysed here was the final one of the day, a bean-shaped plasma with the largest injected ICRF power. Since signal-to-noise levels with FIDA are low and the Faraday-cup loss signals integrate all incident ions with energy > 10 keV, there is significant uncertainty regarding the particular fast-ion orbits participating in the supposed mode-particle resonance. The data are consistent with the hypothesis that RF-accelerated beam ions are displaced through resonances with the mode, but we cannot exclude orbit stochasticity due to multiple overlapping modes. The results are inconclusive but intriguing, and various diagnostic improvements since the 2010 experiment make this a valuable research topic to revisit.

5. AEs on DIII-D

In DIII-D experiments with NBI during the current-ramp phase of the discharge, various types of AE activity are observed. In these discharges as the current profile evolves, the most common types of MHD activity reported are TAE and reversed-shear AEs (RSAE). Figure 8(*a*) shows the signal from an external magnetic probe during the current-ramp phase of a discharge with strong AE activity where large beam-ion losses are observed. NBI starts at $t = 300$ ms concurrent with the appearance of multiple mode activity, evidenced by the crosspower of two external magnetic probes (figure 8(*b*)). Two main types of AEs are observed; TAEs are identified as having relatively constant frequency evolution while RSAEs have the characteristic of chirping frequency spectra. In this discharge, the AEs are observed at frequencies mainly above 50 kHz; the lower frequency mode evolving from about 10 kHz up to about 30 kHz is a $n = 0$ energetic particle induced geodesic acoustic mode (EGAM) [57] and is not associated with AE activity. However, EGAMs are observed to cause coherent beam-ion losses [58], which will be discussed in detail in future publications.

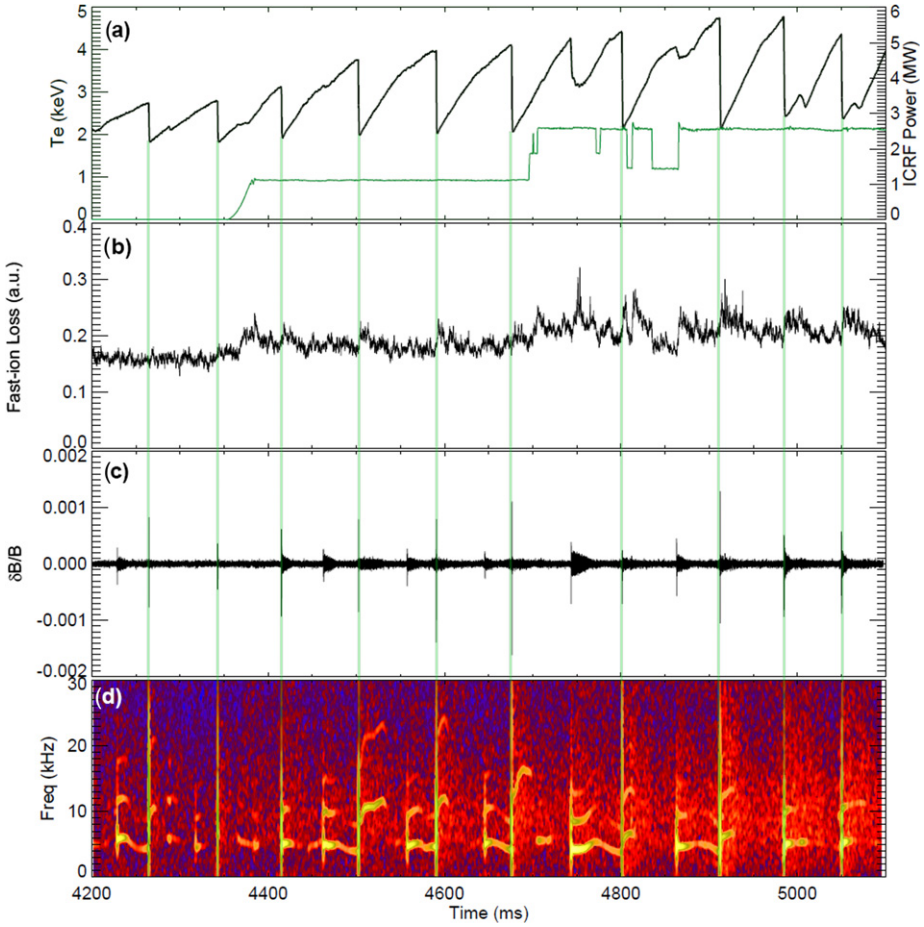

Figure 6. Time history during several sawtooth cycles of (*a*) core electron temperature (black) and ICRF power (green), (*b*) fast-ion loss signal measured by a Faraday-cup detector, (*c*) external magnetic probe signal and (*d*) crosspower of two magnetic probes separated toroidally. The faint vertical lines indicate the sawtooth crashes that were evaluated in this paper.

During strong TAE and RSAE activity, the neutron rate is suppressed up to 50% compared with classical predictions, implying strong transport of beam ions [54]. High-bandwidth FILD measurements indicate losses coherent with AE fluctuations. Analysis of the pitch- and energy-resolved FILD measurements show that the losses are from nearly full-energy (∼75 keV) beam ions with pitch ($v_\parallel/v$) about 0.7 [58]. Mode-induced loss of beam ions results from resonances with the modes, kicking particles into loss boundaries. Because the frequency of the AEs are typically quite high, losses can be associated with a multitude of high-harmonic mode-particle resonances. Figure 9 represents the zoology of resonance curves in velocity space due to a single mode ($n = 2$, $f = 70$ kHz at $t = 448$ ms) at the approximate radial location of the peak of the mode amplitude ($r/a \approx 0.3$). While resonant losses of all classes of particles may be possible, the losses observed are likely due to counter-passing fast ions. We can see why from figure 9. Numerous resonances converge near the counter-passing/lost-particle boundary. Ions can undergo a change in their energy and canonical toroidal momentum when interacting resonantly with a mode. The magnitude of the change depends on the amplitude of the mode, and for small amplitude perturbations such as AEs, a single resonant interaction minimally changes the particle's constants of motion. However, a fast ion in a region of velocity space with closely spaced resonances can interact with the mode multiple times leading to a significant modification to its orbit.

Simulations of the DIII-D data confirm that the AE and particle undergo multiple interactions, reducing the canonical toroidal momentum of counter-passing ions, leading consequently to a reduction in $v_\parallel$, and transforming them to trapped ions on loss orbits. The simulations model the observed losses and reproduce the pitch and energy distribution of lost beam ions. The simulation procedure involves several steps which are outlined here. First, the linear eigenfunctions are calculated by the ideal MHD solver NOVA [59, 60] from supplied EFIT [40] equilibrium and plasma profile data. The eigenfunctions are fit to those measured by the ECE diagnostics [46, 61] and assigned amplitudes corresponding to the measured values. The Hamiltonian guiding-centre code ORBIT [62] is used to follow the particle distribution through the equilibrium fields perturbed by the NOVA-supplied wave fields. Particle orbits crossing the last-closed flux surface are traced by a second guiding-centre code employing the constants of motion (appendix of [54]). Particles that strike the position of the FILD detector are recorded. The simulation accurately predicts the energy distribution of lost fast ions and models the pitch-angle distribution within 10% of the measurement. The interested reader is referred to [54, 58]

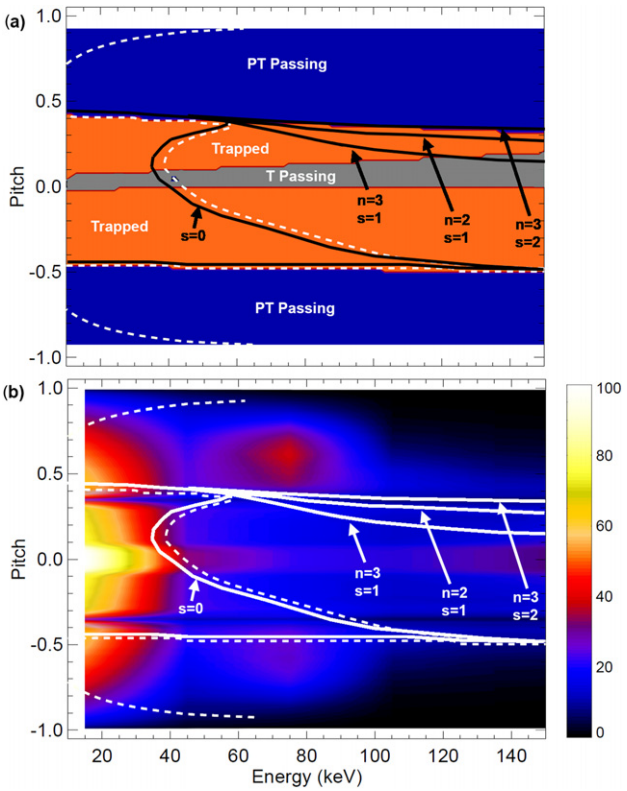

Figure 7. Velocity-space plot at $R = 193$ cm and midplane of (a) orbit classification (PT passing—poloidally and toroidally passing ions, T Passing—toroidally passing, poloidally trapped ions, Trapped—poloidally and toroidally trapped ions) and (b) fast-ion distribution function for NBI+ICRF. The critical energy for flux attachment (E_{crit}) is denoted with the dashed lines. The sawtooth-relevant resonance curves (for $f = 6$ kHz) are plotted as solid lines.

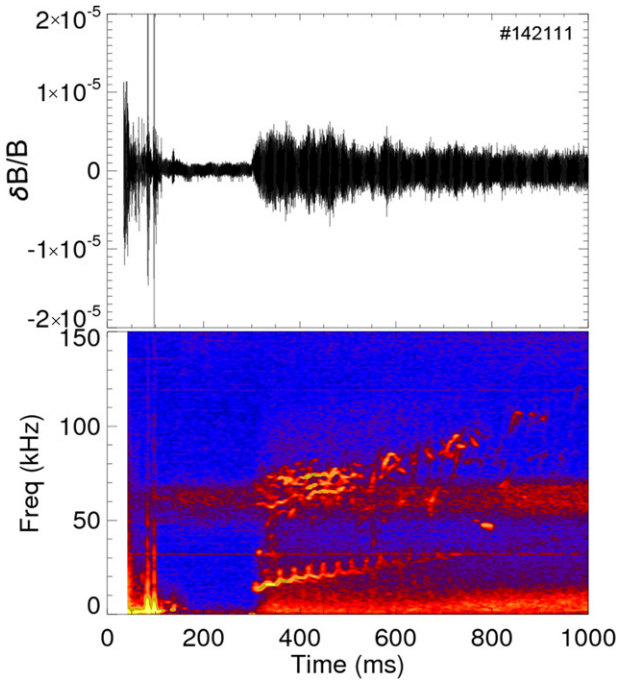

Figure 8. Time history of (a) external magnetic probe during TAE and RSAE activity, and (b) crosspower of two magnetic probes separated toroidally.

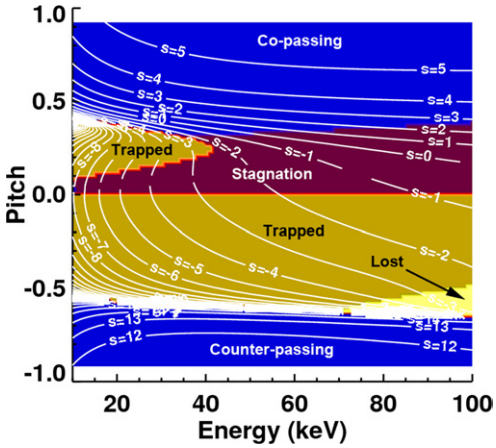

Figure 9. Velocity-space plot of orbit classifications and resonance curves pertaining to $n = 2$, $f = 70$ kHz TAE, evaluated at the spatial position near the peak of the eigenfunction.

for details regarding DIII-D's measurements of fast-ion losses induced by AEs.

6. Summary

The DIII-D program has recently commissioned several new fast-ion diagnostics, including measurements of both the confined *and* lost populations. Results from three classes of experiments were discussed to disseminate our current understanding of the dynamic process of fast-ion transport during a variety of MHD instabilities. In the three examples presented here (fishbones, sawteeth and Alfvén eigenmodes), the common theme involves mode-particle resonances, despite the disparities among the different types of instabilities. Although these instabilities encompass a broad range of frequencies and mode structures, significant modifications to the fast-ion distribution function ensue. Low-frequency kink-like instabilities with large-amplitude magnetic perturbations (e.g. fishbones and sawteeth) as well as high-frequency wave-like instabilities with small magnetic perturbations (e.g. AEs) can interact with different parts of the fast-ion distribution function. The magnitude of particle transport (either convective or diffusive) depends on the mode amplitude. For large-amplitude modes, a single interaction between the mode and a particle can lead to large orbit excursions, made possible through a change in the particle's energy and/or through a change in the particle's canonical momentum. Smaller-amplitude modes are less effective at driving transport. However, as seen for AEs, a region of phase space with a dense concentration of resonances can lead to multiple small changes to the particle's energy and canonical momentum, culminating into a major orbit transformation. DIII-D research on mode-particle resonances is ongoing. In conjunction with DIII-D FIDA data, a proposed collaboration would investigate predicted levels of fast-ion transport at a sawtooth crash with the self-sufficient fluid-kinetic hybrid model M3D [63]. Efforts are also underway to extrapolate fast-ion losses by AEs in ITER. Also, mode-particle resonances in the presence of neoclassical tearing modes will be the

subject of future work. Advances in our understanding of transport phenomena will hopefully motivate experimental and theoretical collaborations. As we approach the ITER era, we will ultimately require capabilities to predict accurately transport fluxes under a variety of conditions.

Acknowledgments

Helpful discussions with R.K. Fisher, Y.I. Kolesnichenko, V.V. Lutsenko, B.J. Tobias, R.B. White and Y.V. Yakovenko are gratefully acknowledged. Furthermore, a special thanks to the DIII-D team for their incredible assistance on making possible all of the aforementioned experiments.

References

[1] White R.B. 2006 *The Theory of Toroidally Confined Plasmas* (London: Imperial College Press)
[2] Mcguire K. *et al* 1983 *Phys. Rev. Lett.* **50** 891
[3] Chen L., White R.B. and Rosenbluth M.N. 1984 *Phys. Rev. Lett.* **52** 1122
[4] White R.B. *et al* 1983 *Phys. Fluids* **26** 2958
[5] Jarvis O.N. *et al* 1996 *Nucl. Fusion* **36** 1513
[6] Kolesnichenko Y.I. and Yakovenko Y.V. 1996 *Nucl. Fusion* **36** 159
[7] Kolesnichenko Y.I., Lutsenko V.V. and Yakovenko Y.V. 1998 *Phys. Plasmas* **5** 729
[8] Duong H.H. *et al* 1993 *Nucl. Fusion* **33** 749
[9] Garcia-Munoz M. *et al* 2010 *Nucl. Fusion* **50** 084004
[10] Pinches S.D. *et al* 2006 *Nucl. Fusion* **46** S904
[11] Garcia-Munoz M. *et al* 2011 *Nucl. Fusion* **51** 103013
[12] Carolipio E.M. *et al* 2002 *Nucl. Fusion* **42** 853
[13] Garcia-Munoz M. *et al* 2007 *Nucl. Fusion* **47** L10
[14] Mynick H.E. 1993 *Phys. Fluids* B **5** 1471
[15] Heidbrink W.W. *et al* 2004 *Plasma Phys. Control. Fusion* **46** 1855
[16] Luo Y. *et al* 2007 *Phys. Plasmas* **14** 112503
[17] Muscatello C.M. *et al* 2012 *Plasma Phys. Control. Fusion* **54** 025006
[18] Luo Y., Heidbrink W.W. and Burrell K.H. 2004 *Rev. Sci. Instrum.* **75** 3468
[19] Heidbrink W.W. *et al* 2008 *Rev. Sci. Instrum.* **79** 10E520
[20] Muscatello C.M. *et al* 2010 *Rev. Sci. Instrum.* **81** 10D316
[21] Van Zeeland M.A., Heidbrink W.W. and Yu J.H. 2009 *Plasma Phys. Control. Fusion* **51** 055001
[22] Grierson B.A. *et al* 2012 *Phys. Plasmas* **19** 056107
[23] Grierson B.A. *et al* 2010 *Rev. Sci. Instrum.* **81** 10D735
[24] Heidbrink W.W. *et al* 2007 *Plasma Phys. Control. Fusion* **49** 1457
[25] Garcia-Munoz M. 2006 Fast response scintillator based detector for MHD induced energetic ion losses in ASDEX Upgrade *PhD Thesis* Ludwig-Maximillian-University of Munich
[26] Zweben S.J. 1989 *Nucl. Fusion* **29** 825
[27] Fisher R.K. *et al* 2010 *Rev. Sci. Instrum.* **81** 10D307
[28] Pace D.C. *et al* 2010 *Rev. Sci. Instrum.* **81** 10D308
[29] Heidbrink W.W., Taylor P.L. and Phillips J.A. 1997 *Rev. Sci. Instrum.* **68** 536
[30] Carolipio E.M. and Heidbrink W.W. 1997 *Rev. Sci. Instrum.* **68** 304
[31] Pickering L., Heidbrink W.W. and Zhu Y. 2006 *American Physical Society Division of Plasma Physics (Philadelphia, PA, 2006)* http://adsabs.harvard.edu/abs/2006APS..DPPUP1016P
[32] Okabayashi M. *et al* 2009 *Nucl. Fusion* **49** 125003
[33] Okabayashi M. *et al* 2011 *Phys. Plasmas* **18** 056112
[34] Heidbrink W.W. *et al* 2011 *Plasma Phys. Control. Fusion* **53** 085007
[35] Fonck R.J., Duperrex P.A. and Paul S.F. 1990 *Rev. Sci. Instrum.* **61** 3487
[36] McKee G. *et al* 1999 *Rev. Sci. Instrum.* **70** 913
[37] Kolesnichenko Y.I. *et al* 1997 *Phys. Plasmas* **4** 2544
[38] Kolesnichenko Y.I. *et al* 1998 *Phys. Plasmas* **5** 2963
[39] 1998 Princeton Plasma Physics Laboratory, http://w3.pppl.gov/transp
[40] Lao L.L. *et al* 1985 *Nucl. Fusion* **25** 1611
[41] Pankin A. *et al* 2004 *Comput. Phys. Commun.* **159** 157
[42] Jacquinot J. *et al* 1986 *Plasma Phys. Control. Fusion* **28** 1
[43] Heidbrink W.W. *et al* 1999 *Nucl. Fusion* **39** 1369–89
[44] Pinsker R.I. *et al* 1999 *13th Topical Conf. on Radio Frequency Power in Plasmas (Annapolis, MD, 1999)* pp 144 http://adsabs.harvard.edu/abs/1999AIPC..485..144P
[45] Chapman I.T. 2011 *Plasma Phys. Control. Fusion* **53** 013001
[46] Austin M.E. and Lohr J. 2003 *Rev. Sci. Instrum.* **74** 1457
[47] Kolesnichenko Y.I. *et al* 1992 *Phys. Rev. Lett.* **68** 3881
[48] Porcelli F., Boucher D. and Rosenbluth M.N. 1996 *Plasma Phys. Control. Fusion* **38** 2163
[49] Wesson J.A. 1986 *Plasma Phys. Control. Fusion* **28** 243
[50] Kadomtsev B.B. 1975 *Sov. J. Plasma Phys.* **1** 389
[51] Lazarus E.A. *et al* 2007 *Phys. Plasmas* **14** 055701
[52] Papp G. *et al* 2011 *Plasma Phys. Control. Fusion* **53** 065007
[53] Tobias B.J. *et al* 2011 *IEEE Trans. Plasma Sci.* **39** 3022
[54] Van Zeeland M.A. *et al* 2011 *Phys. Plasmas* **18** 056114
[55] Harvey R.W. and McCoy M.G. 2005 Reconstituted in editable form from General Atomics Report *GA-A20978*, 1992 'The CQL 3D Fokker–Planck Code' www.compxco.com/050520_cql3d_manual.pdf
[56] Smirnov A.P. and Harvey R.W. 2003 The GENRAY Ray Tracing Code Report *CompX–2000-01* Ver. 2 http://compxco.com/Genray_manual.pdf
[57] Nazikian R. *et al* 2008 *Phys. Rev. Lett.* **101** 185001
[58] Pace D.C. *et al* 2011 *Plasma Phys. Control. Fusion* **53** 062001
[59] Cheng C.Z. and Chance M.S. 1987 *J. Comput. Phys.* **71** 124
[60] Cheng C.Z. 1992 *Phys. Rep.* **211** 1
[61] Tobias B. *et al* 2010 *Rev. Sci. Instrum.* **81** 10D928
[62] White R.B. and Chance M.S. 1984 *Phys. Fluids* **27** 2455
[63] Park W. *et al* 1999 *Phys. Plasmas* **6** 1796